

Running title: BDE-47 ADSORPTION KINETICS ON MAIZE STRAW BIOCHARS

Adsorption Kinetics of 2,2',4,4'-tetrabromodiphenyl Ether on Maize Straw-derived Biochars

LIU Guangxia^{1,2}, SONG Yang¹, SHENG Hongjie^{1,2}, YE Mao¹, Robert D STEDTFELD³, BIAN Yongrong¹, GU Chenggang¹, JIANG Xin¹, WANG Fang^{1,2,*}

¹ Key Laboratory of Soil Environment and Pollution Remediation, Institute of Soil Science, Chinese Academy of Sciences, Nanjing 210008, China

² University of Chinese Academy of Sciences, Beijing 100049, China

³ Department of Civil and Environmental Engineering, Michigan State University, MI 48824, USA

ABSTRACT

Chars in the natural environment can affect the migration of polybrominated diphenyl ethers (PBDEs). However, research relating adsorption behavior and mechanisms of PBDEs on biochars is lacking. This study examined the adsorption kinetics of 2,2',4,4'-tetrabromodiphenyl ether (BDE-47) on maize straw-derived biochars (MBC) pyrolyzed at four different temperatures via batch experiments. Biochar samples were characterized by Fourier transform infrared (FTIR), Raman spectra and elemental analysis. Two-compartment first-order model and pseudo-second-order model had a better fit compared to pseudo-first-order model in describing the BDE-47 adsorption on biochars, which was dominated by slow adsorption compartment and chemisorption. The MBC pyrolyzed at 600 °C had the greatest adsorption capacity of BDE-47 due to surface area and aromaticity. However, there was no significant difference in the adsorption capacities among three additional biochars. The organic functional groups coupled with graphene structures of biochars and hydrophobic effect promoted the adsorption of BDE-47. Pore diffusion was not the sole rate-limiting step; and film diffusion was also involved in the adsorption process of BDE-47 on biochars. Overall, results demonstrate transport and potential treatment of PBDEs using biochars.

Key Words: adsorption, BDE-47, biochar, kinetics, mechanism

INTRODUCTION

Polybrominated diphenyl ethers (PBDEs) are a widely applied brominated flame retardants (BFRs) (Darnerud *et al.*, 2001), which can enter the environment through the processes of production, recycling and disposal (Ma *et al.*, 2012). As persistent organic pollutants (POPs), PBDEs can exert a potential negative effect on soil, water, atmosphere and biological organisms. PBDEs can induce carcinogenicity, immunotoxicity, liver damage, and can disrupt thyroid homeostasis and oestrogen signal transduction, causing multiple negative health effects (Man *et al.*, 2011). Therefore, effective and eco-friendly technology must be used to immobilize PBDEs and bioavailability in the environment.

To reduce the concentration of PBDEs existed in soil and aquatic environment, many remediation technologies can be adopted, such as bioremediation (Xin *et al.*, 2014), phytoremediation (Li *et al.*, 2018), photodegradation (Li *et al.*, 2008), electrokinetic remediation (Wu *et al.*, 2012), adsorption (Yi *et al.*, 2017) and the combination of persulfate oxidation and chemical washing (Chen *et al.*, 2017). Among these technologies, adsorption has advantages of low cost, simple operation, and effective contaminant control. In addition, adsorption influences migration, degradation and bioavailability of organic pollutants in the natural environment

* Corresponding author. E-mail: wangfang@issas.ac.cn

(Lou *et al.*, 2015; Cheng *et al.*, 2017). Biochars, considered a super adsorbent for hydrophobic organic contaminants (HOCs), are produced from the process of biomass pyrolysis under oxygen limited conditions (Kupryianchyk *et al.*, 2016). During the adsorption process of organic contaminants, pyrolytic temperature is a vital factor influencing the physicochemical property and adsorption capacities of biochars (Chen and Chen, 2009). Current research mainly focuses on PBDEs adsorption on soil particles (Liu *et al.*, 2010; Olshansky *et al.*, 2011), while reports on the adsorption of PBDEs on biochars are rare.

The objective of the present study was to investigate the interactions between PBDE and maize straw biochars pyrolyzed at different temperatures via adsorption batch experiments. This was done to elucidate adsorption capacities, kinetics and determine relevant mechanisms. Maize straw from agricultural wastes was used as a readily available and low-cost resources. 2,2',4,4'-tetrabromodiphenyl ether (BDE-47) was selected as a model congener of PBDEs due to its high environmental concentration and biotoxicity (Richardson *et al.*, 2008). Results provide support in evaluating the mobility and bioavailability of PBDE in the presence of biochars under environmental conditions.

MATERIALS AND METHODS

Chemicals

BDE-47 (98.5% purity) was obtained from Chem Service incorporated company (West Chester, Pennsylvania, USA). Methanol and n-hexane (chromatographic purity) were purchased from Tedia Company (Fairfield, USA). All other reagents and chemicals applied were of analytical pure. Milli-Q water was applied through the whole experiments. The standard stocking solution of BDE-47 in methanol (1000 mg L^{-1}) was stored at $-20 \text{ }^{\circ}\text{C}$.

Preparation and characterization of maize straw biochars

The procedure of producing maize straw biochars with different pyrolyzed temperatures (300, 400, 500 and $600 \text{ }^{\circ}\text{C}$) was in accordance with a previous study (Jia *et al.*, 2013). Briefly, the maize straw were washed with deionized water to remove impurities and oven-dried at $80 \text{ }^{\circ}\text{C}$ for 12 h. Then they were transferred to biochar reactor with oxygen limited conditions. The step wise heating procedure was as follows: The initial temperature was settled at $200 \text{ }^{\circ}\text{C}$, then heated to $250 \text{ }^{\circ}\text{C}$ and eventually to 300, 400, 500 and $600 \text{ }^{\circ}\text{C}$, respectively. The maize straw were pyrolyzed constantly for 1.5 h at each temperature. At the final temperature (300, 400, 500 and $600 \text{ }^{\circ}\text{C}$), the heating procedure was stopped when no further smoke was produced. The obtained biochar samples were grounded and passed through a 100 mesh sieve after cooling. Finally, the biochar samples were further oven-dried 12 h at $70 \text{ }^{\circ}\text{C}$. Then the biochar samples pyrolyzed at 300, 400, 500 and $600 \text{ }^{\circ}\text{C}$ were labeled as MBC300, MBC400, MBC500 and MBC600, respectively.

The elemental composition (C, H and N contents) of different biochar samples were analyzed by a CNH analyzer (Vario MICRO, elemental, Germany). The oxygen content was calculated as follows: $\text{O}\% = 100\% - (\text{C} + \text{H} + \text{N} + \text{ash})\%$ (Fuertes *et al.*, 2010). The ash content was determined as the remaining mass after combusting biochars to constant weight at $750 \text{ }^{\circ}\text{C}$. The organic functional groups on biochars surface were quantified by Boehm titration method (Boehm, 1994). The assumptions are as follows: all acidic and basic groups can be neutralized by NaOH and HCl, respectively. NaHCO_3 can only neutralize carboxyl groups, while Na_2CO_3 neutralizes carboxyl and lactonic groups. The specific surface area and pore distributions were measured with a surface area analyzer (ASAP-2020, Micromeritics, USA) using nitrogen gas adsorption method. Functional groups on biochars surface were recorded using a NEXUS 870 spectrophotometer (Thermo Nicolet, USA) for Fourier transform infrared spectroscopy (FTIR) analysis. Raman spectra of the biochar samples were analyzed with InVia laser Raman spectrometer (Renishaw, UK).

Adsorption kinetic experiments

Batch adsorption experiments were performed in 20 mL brown glass bottles (teflon caps) with biochars (1 mg), BDE-47 (1 mg L^{-1}), CaCl_2 (0.01 mol L^{-1} , to retain relative stable ion strength) and HgCl_2 (100 mg L^{-1} , to restrain microbial activity) were added. The total volume was settled as 20 mL to remain the headspace of every bottle small enough and to decrease the possible volatilization of BDE-47. Blank controls without adsorbents (biochars) were also conducted to evaluate the BDE-47 volatilization and possible adsorption of

BDE-47 on glass bottles. Glass bottles were placed in a Rolldrum shaker (WH-962, Taicang, China) at 25 °C and 30 rpm, then the bottles were sacrificed for the analysis of BDE-47 at different time points of 0.5, 1, 2, 4, 9, 24, 48 h.

Analysis of BDE-47

Suction filtration with glass fiber film (0.22 µm) was adopted to separate the biochar samples (solid phase) and the reaction solution (liquid phase) after the experiment. After filtering, glass bottles were washed twice with 10 mL Milli-Q water and the washing solution were also filtrated through the same film. BDE-47 existed in filtrate and that may be adsorbed on the glass bottle walls were extracted by 10 mL n-hexane (vortex 2 min), respectively. Then the two parts n-hexane phases (20 mL) were vortexed together (2 min) and served as the part of BDE-47 that not be adsorbed by biochars. The concentration of BDE-47 in n-hexane was quantified by gas chromatography (GC) after dehydrating with anhydrous sodium sulfate.

The GC (Agilent 6890, USA) was equipped with a DB-5 chromatographic column (30 m length × 0.32 mm inside diameter × 0.25 µm film thickness), a ⁶³Ni electron capture detector and a HP 7683 auto sampler. The oven temperature program was run from 150 to 210 °C at 25 °C min⁻¹ for 6 min, followed by a ramp up of 5 °C min⁻¹ to 260 °C (held for 1 min), then to 280 °C at 15 °C min⁻¹ for 5 min and ultimately to 300 °C at 15 °C min⁻¹ for 2 min. The carrier gas N₂ (99.999%) was applied at a flow rate of 1.9 mL min⁻¹.

FTIR analysis

The functional groups on biochar surfaces were determined with FTIR before and after adsorption of BDE-47. There were eight treatments as follows: (a) MBC300, (b) MBC400, (c) MBC500, (d) MBC600, (e) MBC300-BDE47, (f) MBC400-BDE47, (g) MBC500-BDE47, (h) MBC600-BDE47. After adsorption equilibrium of BDE-47 was achieved at 48 h, the biochar samples were separated and collected for FTIR analysis. The freeze-dried biochar samples (1 mg) were mixed with oven-dried KBr (200 mg, 105-110 °C). Then the mixture were pressed into a pellet to record FTIR spectrum.

Adsorption kinetic models

The adsorption kinetic process was elaborated using pseudo-first-order, pseudo-second-order, two-compartment first-order and intra-particle diffusion models.

The pseudo-first-order kinetics model assumes uniform and monolayer adsorption process (Gong *et al.*, 2017) and is described as:

$$q_t = q_e(1 - e^{-k_1 t})$$

Where q_t (mg g⁻¹) is the quantity of BDE-47 adsorbed on biochars at time t (h); q_e (mg g⁻¹) represents BDE-47 adsorption capacity at equilibrium and k_1 (h⁻¹) is the pseudo-first-order model rate constant.

The pseudo-second-order kinetics model implies chemical adsorption related to electronic forces (Qiu *et al.*, 2009) and is expressed as:

$$q_t = \frac{q_e^2 k_2 t}{1 + q_e k_2 t}$$

Where q_t (mg g⁻¹) is the quantity of BDE-47 adsorbed on biochars at time t (h); q_e (mg g⁻¹) represents BDE-47 adsorption capacity at equilibrium and k_2 (g mg⁻¹ h⁻¹) is the rate constant of pseudo-second-order model.

The two-compartment first-order model assumes that the adsorption process is composed of a fast and slow compartment and the two compartments proceed simultaneously (Pan *et al.*, 2006; Fang *et al.*, 2014).

$$q_t = q_f(1 - e^{-k_f t}) + q_s(1 - e^{-k_s t})$$

Where q_t (mg g⁻¹) represents the adsorption quantity of BDE-47 on biochars at time t (h); q_f (mg g⁻¹) is the BDE-47 adsorption quantity of fast compartment; q_s (mg g⁻¹) is the BDE-47 adsorption quantity of slow compartment; k_f and k_s (h⁻¹) represent the fast and slow rate constant, respectively. $q_t + q_f = q_e$ (q_e , equilibrium adsorption capacity).

In general, the mechanisms of adsorption process could be divided into four steps: bulk diffusion, film diffusion, pore diffusion (or intra-particle diffusion) and adsorbate adsorbed on the adsorbent surface. With the existence of adsorbent (biochar), bulk diffusion was not involved in present study. Adsorbate adsorbed on the adsorbent surface is a fast process and is not the rate-limiting step. Thus, the rate-limiting step mainly depends

on either film or pore diffusion (Güzel *et al.*, 2014).

Intra-particle diffusion model is widely applied to identify the rate-limiting step in adsorption kinetic process and it is defined as:

$$q_t = k_p t^{0.5} + C$$

Where k_p ($\text{mg g}^{-1} \text{h}^{-0.5}$) represents the rate constant of intra-particle diffusion model; C (mg g^{-1}) represents constant that definite the thickness of boundary layer. If the lines of intra-particle diffusion model pass through the origin then pore diffusion is the only rate-limiting step.

The root mean square error (RMSE) represents the goodness of model fit and are expressed as:

$$\text{RMSE} = \sqrt{\frac{\sum_{i=1}^n (q_{i,\text{exp}} - q_{i,\text{mod}})^2}{n}}$$

Where $q_{i,\text{exp}}$ (mg g^{-1}) is the value of BDE-47 quantity adsorbed on biochars from the batch experiment; $q_{i,\text{mod}}$ (mg g^{-1}) is the value of BDE-47 quantity adsorbed on biochars calculated from adsorption kinetic models; n is the number of observations in the adsorption kinetic models. The smaller the RMSE value is, the better the model curve fits.

RESULTS AND DISCUSSION

Surface characterization of maize straw-derived biochars

The specific surface area of the maize straw biochars pyrolyzed at different temperature ranged from 0.48 to 3.15 $\text{m}^2 \text{g}^{-1}$ and 600 °C biochar had the highest surface area (TABLE I). Compared to biochars reported by other studies (Son *et al.*, 2018; Zhou *et al.*, 2018), the surface areas of obtained biochars were relatively low, which might be due to the different production procedure and biomass resources. The results of elements composition showed that maize straw biochars featured high carbon content from 60.00% to 80.50% and MBC600 had the highest carbon content of 80.50% (TABLE I). However, MBC600 had the lowest oxygen content of 10.36% and lowest content of hydrogen (1.30%). The relatively higher oxygen contents were observed in low and medium biochars (MBC300, 400 and 500), showing the presence of abundant oxygen or oxygen-containing functional groups. Hydrogen carbon ratio (H/C) and (O+N)/C atomic ratio indicate the aromaticity and polarity of biochar surface, respectively. In general, the values of H/C and (O+N)/C decreased with the increase of pyrolysis temperature, indicating MBC600 had the highest aromaticity and the lowest polarity. The characteristic results of MBC300 and MBC600 were similar with our previous study (Jia *et al.*, 2016). Different pyrolyzing temperatures generated different carbonization features and elements composition, while the physicochemical property of MBC300, 400 and 500 had little differences. In addition, phenol hydroxyl, carboxyl and lactones base were abundant in MBC300 and MBC400, whereas lactones base disappeared in MBC500 and carboxyl vanished in MBC600 (TABLE I).

Raman spectra can be applied to analyze the carbon structure with ordered or disordered layers. Raman spectroscopy of all biochar samples demonstrated two prominent peaks (Fig. 1): D band associated with the existence of disordered carbon structure with defects ($1300\text{-}1400 \text{ cm}^{-1}$), which may be generated by the decomposition of amorphous organic matter during pyrolyzed process of biochars (Mendonca *et al.*, 2017). The G band was composed of more ordered and less defective graphene structures ($1500\text{-}1600 \text{ cm}^{-1}$). The results of Raman spectra indicated the existence of graphene like structures of biochar samples (Jia *et al.*, 2016). I_D/I_G ratios, calculated from the intensities of D and G bands, represent ratios of disordered/ordered graphene structures. The I_D/I_G values were 0.79, 0.79, 0.67 and 0.73 for MBC300, MBC400, MBC500 and MBC600, respectively, indicating that MBC500 and MBC600 had relatively higher content of ordered graphene structures, while more disordered defective graphene structures were formed in MBC300 and MBC400.

Effect of contact time on adsorption and adsorption kinetics

The contact time in adsorption kinetic process can be used to determine the optimum time for adsorbates to reach maximum adsorption quantity, which had significant effect on practical application of biochars. In general, the amount of adsorbed BDE-47 on all the maize straw-derived biochars pyrolyzed at different temperature increased with the prolongation of contact time period between the biochar and the chemical (Fig. 2a, b). During the initial 2 h, there was a faster adsorption of BDE-47 on biochars and approximately 37.65-

46.38% of BDE-47 was adsorbed. The rapid adsorption of BDE-47 could be ascribed to the large number of empty activated adsorption sites on biochars and the strong adsorption affinities between adsorbates and adsorbents. This rapid adsorption was followed by a moderate increase of BDE-47 adsorbed on biochars. Ultimately, the adsorption of BDE-47 achieved a balance after reaching the saturated adsorption quantities of the biochars. The apparent equilibrium for the adsorption of BDE-47 on biochars with four different pyrolyzed temperatures was obtained at 48 h. MBC600 had a higher equilibrium adsorption amount of BDE-47 (22.57%) compared with other three biochars (MBC300, MBC400 and MBC500), whereas there was no significant difference in equilibrium adsorption amounts of BDE-47 among the three biochar samples. This results may be attributed to the differences of specific surface area, surface functional groups and carbon phase between the four biochars pyrolyzed at different temperatures. However, the principal factor that governed the differences of BDE-47 adsorption amounts between MBC600 and other three biochars should be further explored.

Adsorption mechanism of BDE-47 on biochars can be obtained by analyzing experimental data with different kinetic models. For all the biochars with four different pyrolyzed temperatures, the fitting of two-compartment first-order model and pseudo-second-order kinetic model obtained relatively higher correlation coefficients (R^2 , 0.92-0.99) and lower root mean square error (RMSE, 0.85-2.19) compared to pseudo-first-order kinetic model (TABLE II, Fig. 2a, b), suggesting that the two-compartment first-order model and pseudo-second-order kinetic model could describe the adsorption kinetic process of BDE-47 on biochars more accurately than pseudo-first-order kinetic model. The better fit results of two-compartment first-order model indicated that fast and slow adsorption compartments were involved in the adsorption process of BDE-47 on biochars. The adsorption rates of the fast compartment (k_f) were higher than that of the slow compartment (k_s) (TABLE II). However, the adsorption capacities of slow compartment (q_s) were significantly higher than that of fast compartment (q_f), indicating that the slow compartment controlled the adsorption kinetic process. In addition, the experimental data fitted well into pseudo-second-order model suggested that chemisorption involving covalent forces through sharing or exchange of electrons occurred in the adsorption process (Wang, 2018). This conclusion was in consistent with the results of FTIR (Fig. 3). Therefore, the adsorption kinetic process of BDE-47 on biochar samples were co-dominated by chemisorption and slow compartment.

To determine the diffusion mechanism of the adsorption kinetic process of BDE-47 adsorbed on biochars, the intra-particle diffusion model was applied to describe the experimental data. The fitting results of intra-particle diffusion model indicated the adsorption kinetic process of BDE-47 on biochars displayed multi-linearity and could be divided into three stages (Fig. 2c). At the first stage (initial 1 h), a very rapid adsorption of BDE-47 is observed on the biochars. The first stage indicated the adsorption of BDE-47 onto the available external surface of biochars (dominated by boundary layer diffusion or external liquid film diffusion), while the second linear stage is attributed to intra-particle diffusion (or pore diffusion) (Zhan *et al.*, 2013). In this stage, the BDE-47 molecules adsorbed onto the active sites of the biochars internal surface and belong to the slow adsorption process. Initially, the contribution of the first stage (fast compartment) was dominant in the adsorption kinetic process of BDE-47 on biochars. Subsequently, the contribution of the second stage (slow compartment) increased slowly and the process of fast compartment decreased accordingly. Until both of the fast and slow compartments remained relatively stable, the sorption of BDE-47 reached an equilibrium at third stage due to the decrease of adsorption sites on biochars. The intercept of the second stage lines provide an estimate of the effect of the boundary layer. The intercept of the second stage is not zero, indicating the participation of the boundary layer diffusion (or external liquid film diffusion). The lines of intra-particle diffusion model did not pass through the origin over the whole time range, therefore pore diffusion was not the sole rate-limiting step and some degree of boundary layer diffusion (external liquid film diffusion) may be involved in the adsorption process. Pore diffusion and film diffusion may control the adsorption of BDE-47 on biochars simultaneously.

FTIR analysis

To better understand the interactions of maize straw biochars prepared at different pyrolysis temperatures and BDE-47 molecules, FTIR analysis was conducted. The results of FTIR spectra (Fig. 3) demonstrated that the OH vibration (3390 cm^{-1}), aliphatic CH_3 asymmetric and symmetric stretching vibration (2954 and 2847 cm^{-1}), the stretching vibration of C-H bond in aromatic structures and heteroaromatic compounds (2924 , 800 - 600 cm^{-1}) (Hossain *et al.*, 2011), stretching of C-O, aromatic-O (1400 - 1200 cm^{-1}) (Mulligan *et al.*, 2010), phenolic OH (1450 cm^{-1}) (Xin *et al.*, 2013), C-O-C (1150 cm^{-1}) (Shen *et al.*, 2018), aromatic C=C stretching and C=O stretching of conjugated ketones and quinones (1600 - 1570 cm^{-1}) (Wang *et al.*, 2013), C-H bending

associated with aromatic out-of-plane deformation (875 and 762 cm^{-1}) (Huang *et al.*, 2018) were rich in MBC300, MBC400 and MBC500, while the aliphatic $-\text{CH}_n$ disappeared and the contents of the other functional groups decreased in MBC600. After adsorbing BDE-47, the peaks near 1300 cm^{-1} were shifted in biochars. These peaks were assigned to ether structures (Shin *et al.*, 1997) and could be the main functional groups of BDE-47 molecule structure, indicating that BDE-47 was successfully adsorbed on the biochars surface. In addition, the functional groups such as OH (3390 cm^{-1}), phenolic OH (1450 cm^{-1}), aromatic C=C, C=O (1600-1560 cm^{-1}) and C-O-C (1150-1090 cm^{-1}) shifted with the existence of BDE-47. Especially, the intensities of peaks at 1100 cm^{-1} (related to C-O-C functional groups) significantly decreased after BDE-47 interacted with 300 °C, 400 °C and 500 °C biochars. However, this phenomenon was not obvious in MBC600. The results of FTIR spectra suggested the existence of aromatic compounds with oxygen containing functional groups in carbon structure of biochar samples, which may be involved during the adsorption procedure of BDE-47. The surface oxygen containing groups of biochars showed electrical attraction with BDE-47 molecules (the π structure of BDE-47 was electron deficient) and the π - π interactions may be strengthened. Therefore, relatively abundant organic functional groups on the surface of biochars could create favorable conditions for BDE-47 adsorption.

Adsorption mechanisms

The high adsorption capacity of MBC600 can be ascribed to the relatively high surface area, the increased adsorption sites. After normalizing the adsorption amounts of different contact time by measured surface areas of different biochar samples, MBC600 had the lowest adsorption amount per unit of surface area, while MBC300 had the highest value (Fig. 4). Compared to other three biochar samples, little functional groups were existed in MBC600 due to the high pyrolyzed temperature (Fig. 3). These results indicated that the adsorption amount of MBC600 was primarily dominated by the effect of surface area. The highest adsorption amount per unit surface area of MBC300 may be attributed to the effect of abundant surface functional groups. This phenomenon suggested that the adsorption amounts of MBC300, MBC400 and MBC500 may be controlled by the co-effects of several factors such as surface area (TABLE I), surface functional groups (Fig. 3) and different carbon structure (Fig. 1). In addition, the relatively higher pyrolyzed temperature could also increase the content of carbon phase (TABLE I), thus enhance the surface hydrophobic microenvironment of MBC600 (Fang *et al.*, 2014; Shen *et al.*, 2018). Therefore, BDE-47 with hydrophobic property exhibited high affinities to relatively higher aromatized carbon structure produced at 600 °C. Previous study demonstrated a polydimethylsiloxane (PDMS)-reduced graphene oxide (rGO) chip could adsorb and remove PBDE residues due to both the hydrophobicity and π - π stacking between rGO and PBDE molecules (Chałupniak and Merkoçi, 2017). The molecular dynamics simulation also suggests that PBDE molecules can be adsorbed on graphene structures and the adsorption process is very fast (Ding *et al.*, 2014). Therefore, the relatively high adsorption capacities of biochars may be ascribed to the strong interactions between BDE-47 molecules and graphene structures. In general, maize straw biochars all had relatively high adsorption capacities and affinities for BDE-47.

CONCLUSIONS

The MBC pyrolyzed at 600 °C (MBC600) demonstrated the highest adsorption capacity of BDE-47 compared with low and medium temperature biochars (MBC300, 400 and 500), which had no significant difference in adsorption quantity. The differences in aromaticity and the surface area contributed to the different BDE-47 adsorption capacities on biochars. In addition, the organic functional groups and hydrophobicity also played important roles in the adsorption process. Pore diffusion and film diffusion appeared to be the two main steps controlling BDE-47 adsorption on biochars. This study demonstrates that maize straw biochars (and potentially other high temperature biochars) can be applied as an adsorbent to immobilize PBDEs. In addition, the revealed interactions between BDE-47 and maize straw-derived biochars are beneficial for understanding the fate and transport of PBDEs in the natural ecosystem.

ACKNOWLEDGEMENTS

This study was financially supported by the National Key Basic Research Program of China (No. 2014CB441105), the Outstanding Youth Fund of the Natural Science Foundation of Jiangsu, China

(BK20150050), the National Key Research and Development Program (2016YFD0800204) the National Natural Science Foundation of China (21677149), the Institute of Soil Science, Chinese Academy of Sciences (ISSASIP1616), and the Key Program of Frontier Sciences, Chinese Academy of Sciences (QYZDJ-SSW-DQC035).

REFERENCES

- Boehm H P. 1994. Some aspects of the surface chemistry of carbon blacks and other carbons. *Carbon*. **32**: 759-769.
- Chałupniak A, Merkoçi A. 2017. Toward integrated detection and graphene-based removal of contaminants in a lab-on-a-chip platform. *Nano Research*. **10**: 2296-2310.
- Chen B L, Chen Z M. 2009. Sorption of naphthalene and 1-naphthol by biochars of orange peels with different pyrolytic temperatures. *Chemosphere*. **76**: 127-133.
- Chen F, Luo Z, Liu G, Yang Y, Zhang S, Ma J. 2017. Remediation of electronic waste polluted soil using a combination of persulfate oxidation and chemical washing. *Journal of environmental management*. **204**: 170-178.
- Cheng G H, Sun M Y, Lu J R, Ge X L, Zhang H H, Xu X H, Lou L P, Lin Q. 2017. Role of biochar in biodegradation of nonylphenol in sediment: Increasing microbial activity versus decreasing bioavailability. *Scientific reports*. **7**: 4726.
- Darnerud P O, Eriksen G S, Jøhnnesson T, Larsen P B, Viluksela M. 2001. Polybrominated diphenyl ethers: Occurrence, dietary exposure, and toxicology. *Environ Health Persp* **109**: 49-68.
- Ding N, Chen X F, Wu C-M L. 2014. Interactions between polybrominated diphenyl ethers and graphene surface: A dft and md investigation. *Environ Sci: Nano*. **1**: 55-63.
- Fang C R, Long Y Y, Shen D S. 2014. Sorption behavior of dibutyl phthalate and dioctyl phthalate by aged refuse. *Environmental science and pollution research international*. **21**: 7641-7649.
- Fang Q L, Chen B L, Lin Y J, Guan Y T. 2014. Aromatic and hydrophobic surfaces of wood-derived biochar enhance perchlorate adsorption via hydrogen bonding to oxygen-containing organic groups. *Environmental science & technology*. **48**: 279-288.
- Fuertes A B, Arbustain M C, Sevilla M, Macia-Agullo J A, Fiol S, Lopez R, Smernik R J, Aitkenhead W P, Arce F, Macias F. 2010. Chemical and structural properties of carbonaceous products obtained by pyrolysis and hydrothermal carbonisation of corn stover. *Aust J Soil Res* **48**: 6-7.
- Güzel F, Saygılı H, Saygılı G A, Koyuncu Filiz. 2014. Decolorisation of aqueous crystal violet solution by a new nanoporous carbon: Equilibrium and kinetic approach. *J Ind Eng Chem* **20**: 3375-3386.
- Gong Y P, Ni Z Y, Xiong Z Z, Cheng L H, Xu X H. 2017. Phosphate and ammonium adsorption of the modified biochar based on phragmites australis after phytoremediation. *Environmental science and pollution research international*. **24**: 8326-8335.
- Hossain M K, Strezov V, Chan K Y, Ziolkowski A, Nelson P F. 2011. Influence of pyrolysis temperature on production and nutrient properties of wastewater sludge biochar. *Journal of environmental management*. **92**: 223-228.
- Huang P, Ge C, Feng D, Yu H, Luo J, Li J, Strong P J, Sarmah A K, Bolan N S, Wang H. 2018. Effects of metal ions and ph on ofloxacin sorption to cassava residue-derived biochar. *Science of The Total Environment*. **616-617**: 1384-1391.
- Jia M, Wang F, Bian Y R, Jin X, Song Y, Kengara F O, Xu R K, Jiang X. 2013. Effects of ph and metal ions on oxytetracycline sorption to maize-straw-derived biochar. *Bioresour Technol*. **136**: 87-93.
- Jia M, Wang F, Jin X, Song Y, Bian Y R, Boughner L A, Yang X L, Gu C G, Jiang X, Zhao Q G. 2016. Metal ion-oxytetracycline interactions on maize straw biochar pyrolyzed at different temperatures. *Chem Eng J*. **304**: 934-940.
- Kupryianchuk D, Hale S, Zimmerman A R, Harvey O, Rutherford D, Abiven S, Knicker H, Schmidt H-P, Rumpel C, Cornelissen G. 2016. Sorption of hydrophobic organic compounds to a diverse suite of carbonaceous materials with emphasis on biochar. *Chemosphere*. **144**: 879-887.
- Li H, Li X, Xiang L, Zhao H M, Li Y W, Cai Q Y, Zhu L, Mo C H, Wong M H. 2018. Phytoremediation of soil co-contaminated with cd and bde-209 using hyperaccumulator enhanced by am fungi and surfactant. *Science of The Total Environment*. **613-614**: 447-455.
- Li X, Huang J, Fang L, Yu G, Lin H, Wang L. 2008. Photodegradation of 2,2',4,4'-tetrabromodiphenyl ether in

- nonionic surfactant solutions. *Chemosphere*. **73**: 1594-1601.
- Liu W X, Li W B, Hu J, Ling X, Xing B X, Chen J L, Tao S. 2010. Sorption kinetic characteristics of polybrominated diphenyl ethers on natural soils. *Environmental pollution*. **158**: 2815-2820.
- Lou L P, Yao L D, Cheng G H, Wang L X, He Y F, Hu B L. 2015. Application of rice-straw biochar and microorganisms in nonylphenol remediation: Adsorption-biodegradation coupling relationship and mechanism. *PloS one*. **10**: 1-14.
- Ma J, Qiu X H, Zhang J L, Duan X L, Zhu T. 2012. State of polybrominated diphenyl ethers in china: An overview. *Chemosphere*. **88**: 769-778.
- Man Y B, Lopez B N, Wang H S, Leung A O, Chow K L, Wong M H. 2011. Cancer risk assessment of polybrominated diphenyl ethers (pbdes) and polychlorinated biphenyls (pcbs) in former agricultural soils of hong kong. *Journal of hazardous materials*. **195**: 92-99.
- Mulligan C J, Strezov L, Strezov V. 2010. Thermal decomposition of wheat straw and mallee residue under pyrolysis conditions. *Energy & Fuels*. **24**: 46-52.
- Olshansky Y, Polubesova T, Vetter W, Chefetz B. 2011. Sorption-desorption behavior of polybrominated diphenyl ethers in soils. *Environmental pollution*. **159**: 2375-2379.
- Pan B, Xing B S, Liu W X, Tao S, Lin X M, Zhang Y X, Yuan H S, Dai H C, Zhang X M, Xiao Y. 2006. Two-compartment sorption of phenanthrene on eight soils with various organic carbon contents. *Journal of environmental science and health Part B, Pesticides, food contaminants, and agricultural wastes*. **41**: 1333-1347.
- Qiu H, Lv L, Pan B C, Zhang Q J, Zhang W M, Zhang Q X. 2009. Critical review in adsorption kinetic models. *J Zhejiang Univ-Sc A*. **10**: 716-724.
- Richardson V M, Staskal D F, Ross D G, Diliberto J J, DeVito M J, Birnbaum L S. 2008. Possible mechanisms of thyroid hormone disruption in mice by bde 47, a major polybrominated diphenyl ether congener. *Toxicology and applied pharmacology*. **226**: 244-250.
- Shen J, Huang G, An C J, Xin X Y, Huang C, Rosendahl S. 2018. Removal of tetrabromobisphenol a by adsorption on pinecone-derived activated charcoals: Synchrotron ftir, kinetics and surface functionality analyses. *Bioresource technology*. **247**: 812-820.
- Shin S, Janga J, Yoon S H, Mochidac I. 1997. A study on the effect of heat treatment on functional groups of pitch based activated carbon fiber using ftir. *Carbon*. **35**: 1739-1743.
- Son E B, Poo K M, Chang J S, Chae K J. 2018. Heavy metal removal from aqueous solutions using engineered magnetic biochars derived from waste marine macro-algal biomass. *The Science of the total environment*. **615**: 161-168.
- Wang F. 2018. A novel magnetic activated carbon produced via hydrochloric acid pickling water activation for methylene blue removal. *Journal of Porous Materials*. **25**: 611-619.
- Wang Y, Hu Y, Zhao X, Wang S, Xing G. 2013. Comparisons of biochar properties from wood material and crop residues at different temperatures and residence times. *Energy & Fuels*. **27**: 5890-5899.
- Wu C D, Fan C P, Xie Q J. 2012. Study on electrokinetic remediation of pbdes contaminated soil. *Advanced Materials Research*. **518-523**: 2829-2833.
- Xin J, Liu R, Fan H, Wang M, Li M, Liu X. 2013. Role of sorbent surface functionalities and microporosity in 2,2',4,4'-tetrabromodiphenyl ether sorption onto biochars. *Journal of Environmental Sciences*. **25**: 1368-1378.
- Xin J, Liu X, Liu W, Zheng X-L. 2014. Aerobic transformation of bde-47 by a pseudomonas putida sp. Strain tz-1 isolated from pbdes-contaminated sediment. *Bulletin of Environmental Contamination and Toxicology*. **93**: 483-488.
- Yi Y, Wu J, Wei Y, Fang Z, Tsang E P. 2017. The key role of biochar in the rapid removal of decabromodiphenyl ether from aqueous solution by biochar-supported ni/fe bimetallic nanoparticles. *Journal of Nanoparticle Research*. **19**: 245.
- Zhan Y H, Lin J W, Li J. 2013. Preparation and characterization of surfactant-modified hydroxyapatite/zeolite composite and its adsorption behavior toward humic acid and copper(ii). *Environmental science and pollution research international*. **20**: 2512-2526.
- Zhou L, Richard C, Ferronato C, Chovelon J M, Sleiman M. 2018. Investigating the performance of biomass-derived biochars for the removal of gaseous ozone, adsorbed nitrate and aqueous bisphenol a. *Chem Eng J*. **334**: 2098-2104.

Tables and figures

Tables

TABLE I

The basic physicochemical property of maize straw biochars (MBC) pyrolyzed at 300, 400, 500 and 600 °C.

		MBC300	MBC400	MBC500	MBC600
Ash content (%)		4.77	4.89	5.63	7.16
Elements composition (%)	C	60.00	60.30	62.20	80.50
	H	2.80	2.49	2.05	1.30
	N	2.49	1.30	0.81	0.68
	O	29.94	30.98	29.27	10.36
Molar ratio	H/C	0.56	0.50	0.40	0.19
	O/C	0.37	0.39	0.35	0.09
	(O+N)/C	0.41	0.40	0.36	0.10
Organic functional groups (cmol kg^{-1})	Phenol hydroxyl	352	176	36	45
	Carboxyl	60	14	19	0
	Lactones base	48	41	0	0
S_{BET} ($\text{m}^2 \text{g}^{-1}$)		0.48	1.67	0.84	3.15
Micropore volume ($\text{cm}^3 \text{kg}^{-1}$)		1.92	2.41	3.26	0.90
Median pore width (nm)		0.85	1.41	0.83	1.73

TABLE II

Kinetic parameters of 2,2',4,4'-tetrabromodiphenyl ether (BDE-47) adsorbed on maize straw biochars (MBC) pyrolyzed at 300, 400, 500 and 600 °C.

Biochars	Pseudo-first-order model				Pseudo-second-order model				Two-compartment first-order model						
	q_e (mg g ⁻¹)	k_1 (h ⁻¹)	R^2	RMSE	q_e (mg g ⁻¹)	$k_2 \times 10^2$ (g mg ⁻¹ h ⁻¹) × 10 ²	R^2	RMSE	q_f (mg g ⁻¹)	k_f (h ⁻¹)	q_s (mg g ⁻¹)	k_s (h ⁻¹)	q_e (mg g ⁻¹)	R^2	RMSE
MBC300	21.00±1.49	0.33±0.08	0.93	2.05	23.23±1.31	1.89±0.42	0.97	1.39	8.95±3.64	1.36±0.91	14.02±3.28	0.10±0.06	22.97±0.54	0.98	1.03
MBC400	22.31±0.88	0.29±0.04	0.98	1.18	24.55±1.23	1.58±0.30	0.98	1.24	3.34±4.66	2.01±4.27	19.31±4.47	0.22±0.08	22.65±0.33	0.99	0.93
MBC500	21.94±2.24	0.20±0.06	0.88	2.73	24.06±2.38	1.21±0.44	0.92	2.19	6.79±3.29	2.05±2.39	17.19±3.15	0.08±0.05	23.97±0.37	0.96	1.50
MBC600	28.50±1.41	0.23±0.04	0.97	1.78	31.76±1.31	0.95±0.15	0.99	1.23	6.67±3.17	1.65±1.30	22.97±2.97	0.14±0.04	29.64±0.26	0.99	0.85

Note: RMSE represents root mean square error.

Figures

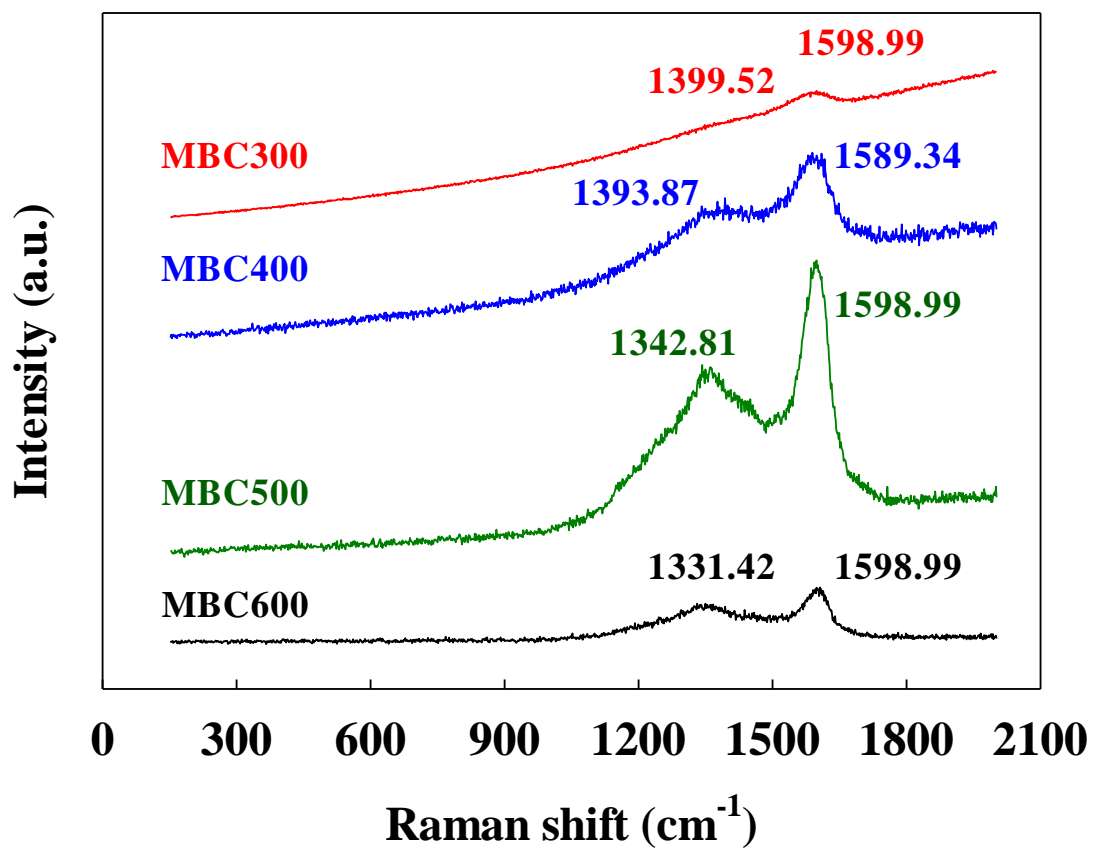


Fig. 1 Raman spectra of maize straw biochars (MBC) pyrolyzed at 300, 400, 500 and 600 °C.

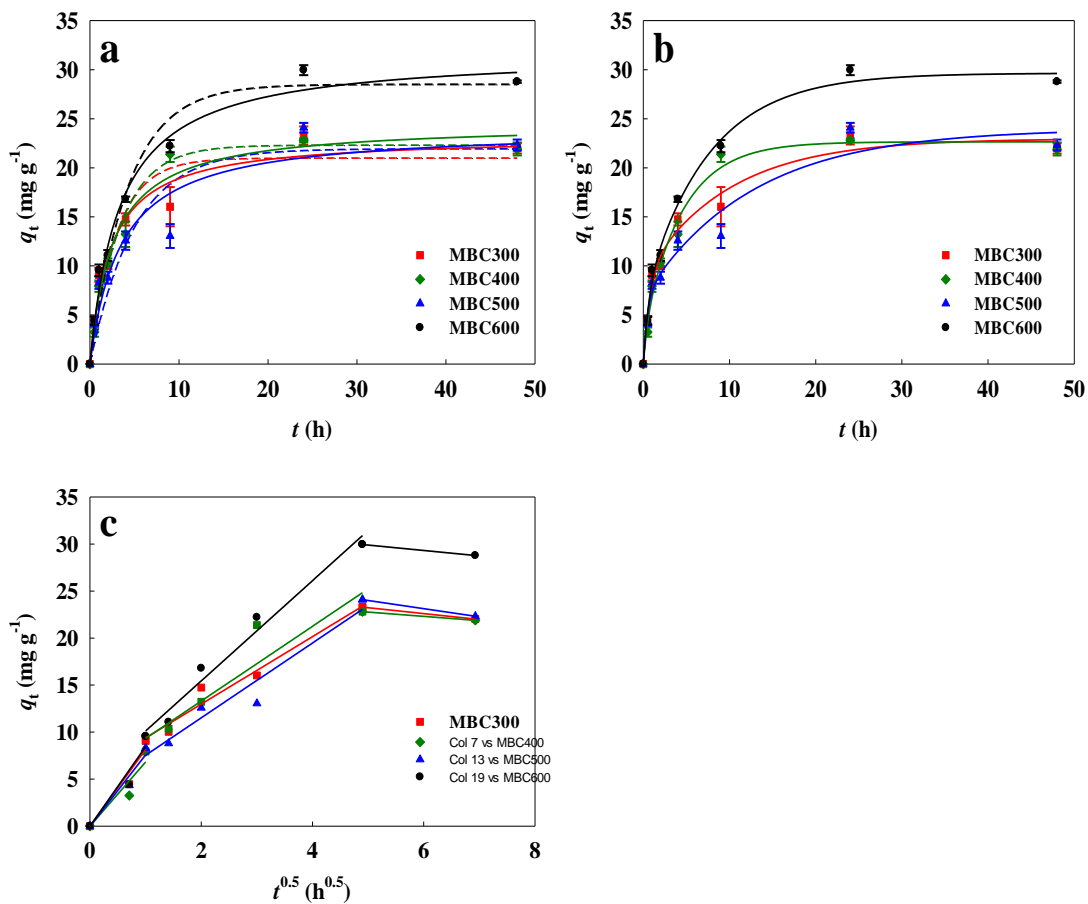


Fig. 2 The plots of pseudo-first-order (a, the dashed curves), pseudo-second-order (a, the solid curves), two-compartment first-order (b) and intra-particle diffusion model (c) of 2,2',4,4'-tetrabromodiphenyl ether (BDE-47) on maize straw biochars (MBC) pyrolyzed at 300, 400, 500 and 600 °C.

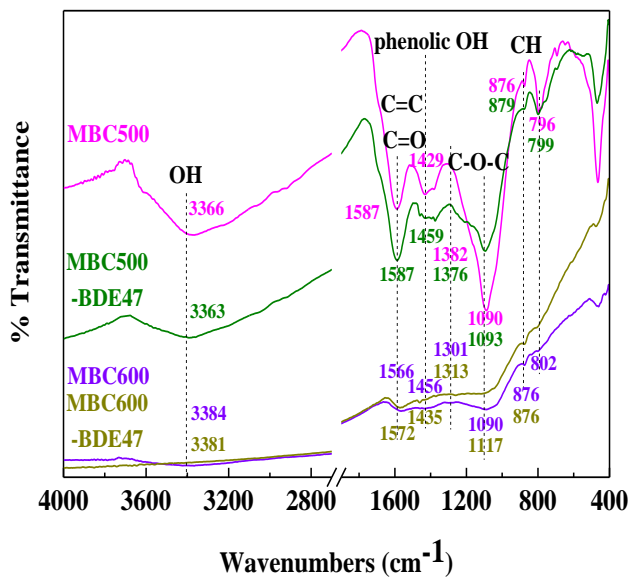
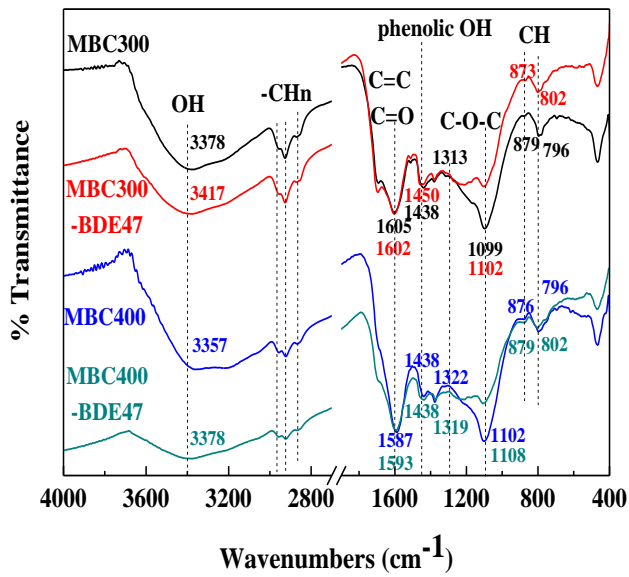


Fig. 3 Fourier transform infrared spectroscopy (FTIR) spectra of maize straw biochars (MBC) pyrolyzed at 300, 400, 500 and 600 °C before and after adsorption of 2,2',4,4'-tetrabromodiphenyl ether (BDE-47).

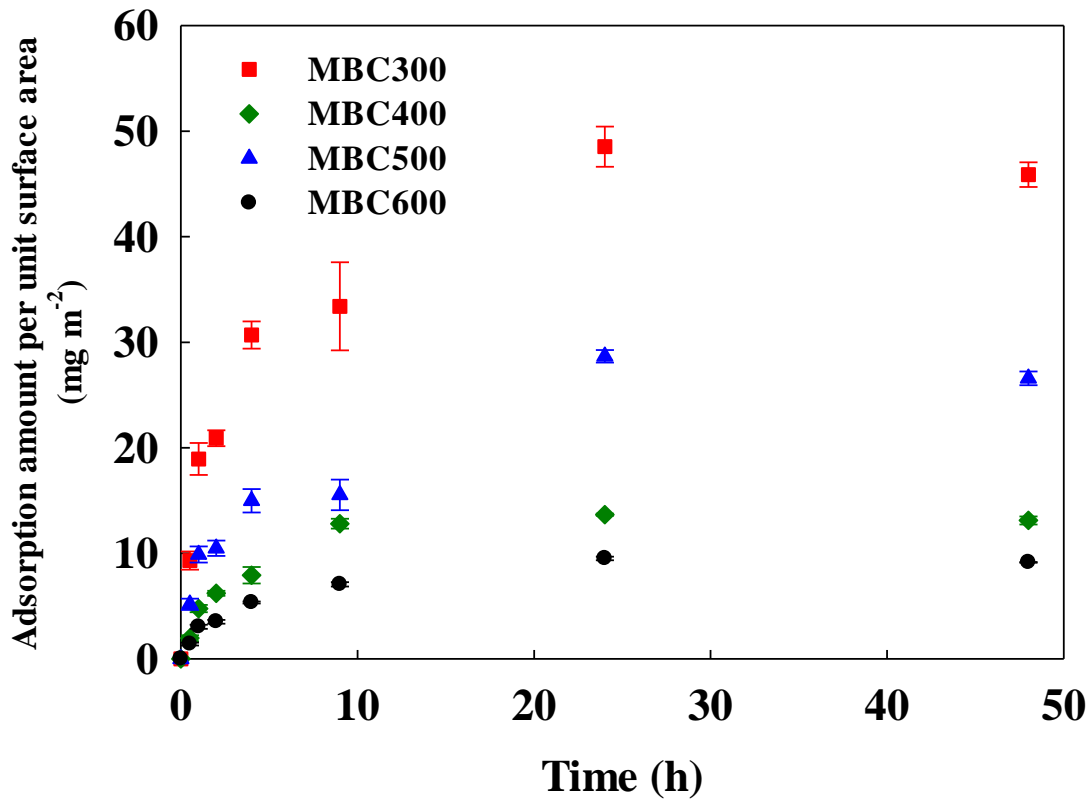


Fig. 4 Adsorption amount per unit surface area of maize straw biochars (MBC) pyrolyzed at 300, 400, 500 and 600 °C varied with contact time.